CO_2 flux over young and snow-covered Arctic pack ice in winter and spring

Daiki Nomura[1, 2, 3*], Mats A. Granskog[4], Agneta Fransson[4], Melissa Chierici[5, 6], Anna Silyakova[7], Kay I. Ohshima[1, 3], Lana Cohen[4], Bruno Delille[8], Stephen R. Hudson[4], and Gerhard S. Dieckmann[9]

1 Institute of Low Temperature Science, Hokkaido University, Kita–19, Nishi–8, Kita–ku, Sapporo, Hokkaido 060–0819, Japan.

2 Faculty of Fisheries Sciences, Hokkaido University, 3–1–1, Minato–cho, Hakodate, Hokkaido 041–8611, Japan.

3 Arctic Research Center, Hokkaido University, Kita–21, Nishi–11, Kita–ku, Sapporo, Hokkaido 001–0021, Japan.

4 Norwegian Polar Institute, Fram Centre, NO–9296 Tromsø, Norway.

5 Institute of Marine Research, NO–9294, Tromsø, Norway.

6 FRAM-High North Research Centre for Climate and the Environment, Tromsø, Norway.

7 CAGE, Centre for Arctic Gas Hydrate, Environment and Climate, Tromsø, Norway.

8 Unité d'Océanographie Chimique, Freshwater and OCeanic science Unit of research, Université de Liège, Liège, Belgium.

9 Alfred Wegener Institute for Polar and Marine Research, Bremerhaven, Germany.

＊Corresponding author: Daiki Nomura, e-mail: daiki.nomura@fish.hokudai.ac.jp,
Faculty of Fisheries Sciences, Hokkaido University, 3–1–1, Minato–cho, Hakodate,
Hokkaido 041–8611, Japan.

Abstract

Rare CO_2 flux measurements from Arctic pack ice show that two types of ice are significant contributors to the release of CO_2 from ice to the atmosphere during winter and spring: young thin ice with thin layer of snow, and old (several weeks) snow covered thick ice. Young thin sea ice is characterized by high salinity and then porosity and thin layer of snow. Snow covered thick ice can remain relatively warm (>–7.5°C) due to a thick insulating snow cover despite air temperatures were as low as –40°C. Brine volume fractions of these two ice type are therefore high enough to provide favorable conditions for gas exchange between sea ice and the atmosphere even in mid-winter. Although the potential CO_2 flux from sea ice decreased due to the presence of the snow, the snow surface is still a CO_2 source to the atmosphere for low snow density and thin snow conditions. We found that young sea ice formed in leads, without snow cover, is the most effective in terms of CO_2 flux (+1.0 ± 0.6 mmol C m^{-2} day^{-1}) since the fluxes are an order of magnitude higher than for snow-covered older ice (+0.2 ± 0.2 mmol C m^{-2} day^{-1}).

1 Introduction

Arctic sea ice is changing dramatically, with rapid declines in summer sea ice extent and a shift towards younger and thinner first-year ice rather than thick multi-year ice (e.g., Stroeve et al., 2012; Meier et al., 2014; Lindsay and Schweiger, 2015). Although the effects of sea ice formation and melting on biogeochemical cycles in the ocean have previously been discussed (e.g., Vancoppenolle et al., 2013), the effects of sea ice freezing and melting on the carbon dioxide (CO_2) exchange with the atmosphere are still large unknowns (Parmentier et al., 2013).

Recent CO_2 flux measurements on sea ice indicate that sea ice is an active component in gas exchange between ocean and atmosphere (Nomura et al., 2013; Geilfus et al., 2013; 2014; Delille et al., 2014; Brown et al., 2015; Kotovitch et al., 2016). The sea-ice CO_2

fluxes depend on (a) the difference in the partial pressure of CO_2 (pCO_2) between the sea ice surface and air, (b) brine volume fraction at the ice-snow interface, (c) ice surface condition including the snow deposited on ice, and (d) wind-driven pressure pumping through the snow. For (a), it is known that the air–sea ice CO_2 flux is driven by the differences in pCO_2 between the sea ice surface and atmosphere (e.g. Delille et al., 2014; Geilfus et al., 2014). The brine pCO_2 changes due to processes within the sea ice, such as thermodynamic process (e.g., Delille et al., 2014), biological activity (e.g., Delille et al., 2007; Fransson et al., 2013; Rysgaard et al., 2013), and calcium carbonate ($CaCO_3$; ikaite) formation and dissolution (e.g., Papadimitriou et al., 2012). When the pCO_2 in the brine is higher than that of the air pCO_2, brine has the potential to release CO_2 to the atmosphere. Brine volume fraction (b) controls permeability of sea ice (Golden et al. 1998) and then CO_2 fluxes (Delille et al. 2014; Geilfus et al 2014). The air–sea ice CO_2 flux is strongly dependent on the sea ice surface conditions (c) (Nomura et al., 2010a, 2013; Geilfus et al., 2013; 2014; Barber et al., 2014; Brown et al., 2015; Fransson et al., 2015). Nomura et al. (2013) proposed that snow conditions (e.g., water equivalent) are important factors affecting gas exchange processes on sea ice. In addition, frost flowers promote CO_2 flux from the ice to the atmosphere (Geilfus et al., 2013; Barber et al., 2014; Fransson et al., 2015). For (d), it is thought that for snow cover, the CO_2 flux is affected by wind pumping (Massman et al.,1995; Takagi et al., 2005) in which the magnitude of CO_2 flux through snow or overlying soil (e.g., Takagi et al., 2005) increases due to wind pumping and can increase the transport relative to molecular diffusion by up to 40% (Bowling and Massman, 2011). These results were mainly found over land-based snow (soil and forest), and thus these processes are not well understood over sea ice (Papakyriakou and Miller, 2011).

In addition to the processes described above, the CO_2 flux over sea ice may also be influenced by the temperature difference between the ice surface and the atmosphere. This has been shown in previous studies in dry snowpacks over land surfaces. These studies show that there is an unstable air density gradient due to heating at the bottom producing a strong temperature difference between bottom and top of snow (e.g., Powers et al., 1985; Severinghaus et al., 2010). This produces air flow within the snowpack, which is a potentially significant contributor to mixing and transport of gas

and heat within the snowpack. We expect that this process would also occur in snow over sea ice, especially during the wintertime when air temperatures are coldest and the temperature difference between sea ice surface (snow bottom) and atmosphere is largest (e.g., Massom et al., 2001). Generally, the sea ice surface under thick snow cover is warm due to the heat conduction from the bottom of sea ice and the insulation effect of the snow cover, and a strong temperature difference between sea ice surface and atmosphere is observed (e.g., Massom et al., 2001). Such a temperature difference would produce an unstable air density gradient and upward transport of air containing CO_2 degassed at the sea-ice surface, thereby enhancing CO_2 exchange between sea ice and atmosphere.

In the ice covered Arctic Ocean, storm periods, with high wind speeds and open leads are important for air-to-sea CO_2 fluxes (Fransson et al., 2017), due to the under-saturation of the surface waters in CO_2 with respect to the atmosphere. On the other hand, the subsequent ice growth and frost flowers formation in these leads promote ice-to-air CO_2 fluxes in winter (e.g. Barber et al., 2014). Given the fact that Arctic sea ice is shrinking and shifting from multi-year ice to first-year ice, the area of open ocean and thinner seasonal ice is increasing. Therefore, the contribution of open ocean/thinner sea ice surface to the overall CO_2 fluxes of the Arctic Ocean is potentially increasing. However, due to the difficulty in acquiring observations over the winter pack ice, most of the winter CO_2 flux measurements were examined over the Arctic landfast ice. Therefore, there is a definite lack of information on conditions during wintertime, especially from Arctic pack ice.

The Norwegian young sea ICE (N-ICE2015) campaign in winter and spring 2015 provided opportunities to examine CO_2 fluxes between sea ice and atmosphere in a variety of snow and ice conditions in pack ice north of Svalbard. Formation of leads and their rapid refreezing allowed us to examine air–sea ice CO_2 fluxes over thin young sea ice, occasionally covered with frost flowers in addition to the snow-covered older ice that covers most of the pack ice area. The objectives of this study were to understand the effects of i) thin sea ice and frost flowers formations on the air–sea ice CO_2 flux in leads, ii) effect of snow-cover on the air–sea ice CO_2 flux over thin, young ice in the

Arctic Ocean during winter and spring seasons, and iii) of the effect of the temperature difference between sea ice and atmosphere (including snow cover) on the air–sea ice CO_2 flux.

2 Materials and Methods

2.1 Study area

This study was performed during N-ICE2015 campaign with R/V Lance in the pack ice north of Svalbard from January to June 2015 (Granskog et al., 2016). Air–sea ice CO_2 flux measurements were carried out from January to May 2015 during the drift of floes 1, 2, and 3 of the N-ICE2015 campaign (Figures 1 and 2, Table 1). The ice pack was a mixture of young ice, first-year ice and second-year ice (Granskog et al., 2017), the two latter with a thick snow cover (Merkouriadi et al., 2017; Rösel et al., 2018). Air–sea ice CO_2 flux measurements were done over young ice (YI stations), first-year ice (FI stations), and old ice (multi-year ice) (OI station). In the N-ICE2015 study region modal ice thickness was about 1.3–1.5 m and modal snow thickness was about 0.5 m (Rösel et al., 2018). Formation of leads and their rapid refreezing provided us the opportunity to examine air–sea ice CO_2 fluxes over thin sea ice, occasionally covered with frost flowers at station YI1 (Figure 2 and Table 1). Air temperature and wind speed were measured at a 10 m weather mast on the ice floe installed about 400 m away from R/V Lance (Cohen et al., 2017).

2.2 CO_2 flux measurements

The air–sea ice CO_2 flux was measured with LI-COR 8100-104 chambers connected to a LI-8100A soil CO_2 flux system (LI-COR Inc., USA) (Figure 2). This enclosed chamber method has been widely applied over snow and sea ice (e.g., Schindlbacher et al., 2007, Geilfus et al., 2015). Two chambers were connected in a closed loop to the infrared gas analyzer (LI-8100A, LI-COR Inc., USA) to measure CO_2 concentration

166 through the multiplexer (LI-8150, LI-COR Inc., USA) with an air pump rate at 3 L min^{-1}
167 . Power was supplied by a car battery (8012-254, Optima Batteries Inc., USA). Four
168 CO_2 standards (324–406 ppmv) traceable to the WMO scale (Inoue and Ishii, 2005)
169 were prepared to calibrate the CO_2 gas analyzer prior to the observations. CO_2 flux was
170 measured in the morning or in the afternoon during low-wind conditions (Table 2), to
171 minimize the effect of wind on the flux (Bain et al., 2005).
172
173 One chamber was installed over undisturbed snow or frost flowers over the ice surface.
174 The chamber collar was inserted 5 cm into the snow and 1 cm into ice at frost flowers
175 site to avoid air leaks between inside and outside of chamber. The second chamber was
176 installed on bulk sea ice after removing the snow or frost flowers. Flux measurements
177 was begun immediately in order to minimize the changes of the ice surface condition. In
178 order to evaluate the effect of removing snow on sea ice surface temperature, ice surface
179 temperature was monitored during CO_2 flux measurements at station FI6. To measure
180 the sea ice surface temperature, temperature sensor (RTR 52, T & D Corp., Japan) was
181 installed in the top of the ice (1 cm) surface after snow removal. During first CO_2 flux
182 measurements (about 30 minutes), ice surface temperature was stable at –5.8°C,
183 suggesting that the effect of removing snow on the variation of sea ice surface
184 temperature was negligible within 30 minutes. The ice surface temperature decreased
185 from –5.8°C to –8.0°C at 200 minutes after removal of snow. Therefore, in this paper,
186 the data of the initial 30 minutes of CO_2 flux measurement after removal of snow or
187 frost flowers was used. The chamber was closed for 20 minutes in a sequence. The 20-
188 minute time period was used because CO_2 fluxes over sea ice are much smaller than
189 over land. The CO_2 concentrations within the chamber were monitored to ensure that
190 they changed linearly throughout the measurement period (example given in Figure 3).
191 The CO_2 flux (mmol C m^{-2} day^{-1}) (positive value indicates CO_2 being released from ice
192 surface to air) was calculated based on the changes of the CO_2 concentration within the
193 headspace of the chamber with LI-COR software (Model: LI8100PC Client v.3.0.1.).
194 The mean coefficient of variation for CO_2 flux measurements was less than 3.0% for
195 CO_2 flux values larger than ±0.1 mmol C m^{-2} day^{-1}. For CO_2 flux values smaller than
196 ±0.1 mmol C m^{-2} day^{-1}, the mean coefficient of variation for CO_2 flux measurements

was higher than 3.0%, suggesting that the detection limit of this system is about 0.1 mmol C m^{-2} day^{-1}.

In this paper, we express the CO_2 flux measured over the snow and frost flowers as F_{snow} and F_{ff}, respectively, and the flux measured directly over the sea ice surface either on snow-free ice or after removal of snow and frost flowers as F_{ice}. F_{snow} and F_{ff} are the natural flux (snow and frost flowers are part of the natural system), and F_{ice} is the potential flux in cases when snow or frost flowers are removed. While removal of snow and frost flowers is an artificial situation, comparisons between F_{ice} and F_{snow} or F_{ff} provide information about the effect of snow on the CO_2 flux. Therefore, in this study, we examine both situations for CO_2 flux.

2.3 Sampling of snow, frost flowers, brine, and sea ice

For salinity measurements, separate samples were taken for snow only, snow and frost flowers, and sea ice surface scrapes. The samples were taken using a plastic shovel, placed into plastic bags and stored in an insulated box for transport to the ship-lab for further processing. Samples were melted slowly (2–3 days) in the dark at +4°C. The temperature of the snow and frost flowers samples were measured during CO_2 flux measurements (approximately 60 minutes after the onset of the CO_2 flux measurement) using a needle-type temperature sensor (Testo 110 NTC, Brandt Instruments, Inc., USA). The accuracy of this sensor is ±0.2°C. Snow density was obtained using a fixed volume sampler (Climate Engineering, Japan) and weight measurement. The depth of the snow pack and frost flowers was also recorded using a ruler.

Brine was also collected at stations FI3–6 for salinity, dissolved inorganic carbon (DIC) and total alkalinity (TA) measurements. Brine was collected from sackholes as described in Gleitz et al. (1995). The sackholes were drilled using a 9 cm diameter ice corer (Mark II coring system, Kovacs Enterprises, Inc., USA) to a depth of 30 cm. The sackholes were then covered with a lid of 5 cm-thick urethane to reduce heat and gas transfer between brine and atmosphere. When brine accumulated at the bottom of the

sackholes (approximately 15 minutes), it was collected with a plastic syringe (AS ONE Corporation, Japan) and kept in 500 mL unbreakable plastic bottles (I-Boy, AS ONE Corporation, Japan) in order to facilitate safe transport to the sampling sites in cold and harsh conditions. The brine bottles were filled without head-space and immediately stored in an insulated box to prevent freezing. Immediately after return to the ship, the brine samples were transferred to 250 mL borosilicate bottles (DURAN Group GmbH, Germany) for DIC and TA measurements using tubing to prevent contact with air. The samples were preserved with saturated mercuric chloride ($HgCl_2$, 60 µL for a 250 mL sample) and stored in the dark at +10°C until analyses was performed at the Institute of Marine Research, Norway.

Sea ice was collected by same ice corer as described for brine collection and at the same location as snow and frost flowers were collected. Sea ice temperature was measured by same sensor as described for snow. For the ice cores, the temperature sensor was inserted in small holes drilled into the core. The core was then cut with a stainless steel saw into 10 cm sections and stored in plastic bags for subsequent salinity measurements. The ice core sections were kept at +4°C and melted in the dark prior to measurement.

2.4 Sample analysis

Salinities for melted snow, frost flowers, sea ice, and brine were measured with a conductivity sensor (Cond 315i, WTW GmbH, Germany). For calibration of salinity measurement, a Guildline PORTASAL salinometer Model 8410A, standardized by International Association for the Physical Sciences of the Oceans (IAPSO) standard seawater (Ocean Scientific International Ltd, UK) was used. Accuracy of this sensor was ±0.003.

Analytical methods for DIC and TA determination are fully described in Dickson et al. (2007). DIC in brine was determined using gas extraction of acidified sample followed by coulometric titration and photometric detection using a Versatile Instrument for the Determination of Titration carbonate (VINDTA 3C, Germany). TA of brine was

261 determined by potentiometric titration of 40 mL sample in open cell with 0.05 N
262 hydrochloric acid using a Titrino system (Metrohm, Switzerland). The average standard
263 deviation for DIC and TA, determined from replicate sample analyses from one sample,
264 was within ±2 μmol kg^{-1} for both DIC and TA. Accuracy of the DIC and TA
265 measurements were ±2 μmol kg^{-1} for both DIC and TA estimated using Certified
266 Reference Materials (CRM, provided by A. G. Dickson, Scripps Institution of
267 Oceanography, USA). The pCO_2 of brine ($pCO_{2\,b}$) was derived from in situ temperature,
268 salinity, DIC and TA of brine using the carbonate speciation program CO2SYS (Pierrot
269 et al., 2006). We used the carbonate dissociation constants (K_1 and K_2) of Mehrbach et
270 al. (1973) as refit by Dickson and Millero (1987), and the KSO_4 determined by Dickson
271 (1990). The conditional stability constants used to derived pCO_2 are strictly only valid
272 for temperatures above 0 °C and salinities between 5 and 50. Studies in spring ice
273 indicated that seawater thermodynamic relationships may be acceptable in warm and
274 low-salinity sea ice (Delille et al., 2007). In sea ice brines at even moderate brine
275 salinities of 80, Brown et al. (2014) found that measured and calculated values of the
276 CO_2 system parameters can differ by as much as 40%. On the other hand, because the
277 CO_2 system parameters are much more variable in sea ice than in seawater, sea ice
278 measurements demand less precision than those in seawater. Fransson et al. (2015)
279 performed one of few detailed analyses of the internal consistency using four sets of
280 dissociation constants and found that the deviation between measured and calculated
281 DIC varied between ±6 and ±11 μmol kg^{-1}, respectively. This error in calculated DIC
282 was considered insignificant in relation to the natural variability in sea ice.
283
284 The pCO_2 of atmosphere was calculated from CO_2 concentration (ppmv) at Ny-Ålesund,
285 Svalbard (http://www.esrl.noaa.gov/gmd/dv/iadv/) taking into account saturated water
286 vapor and atmospheric pressure during sampling day.
287
288 The water equivalent was computed for snow by multiplying snow thickness by snow
289 density (Jonas et al., 2009). Brine volume of sea ice was calculated from the
290 temperature and salinity of sea ice according to Cox and Weeks (1983) and Petrich and
291 Eicken (2010).
292

293

294 # 3 Results

295

296 ## 3.1 Air temperature

297

298 Air temperature is shown in Figure 4. During the study period, air temperature varied
299 significantly from a low of –41.3°C (30 January) to a high of +1.7°C (15 June) (Hudson
300 et al., 2015). Even in wintertime (from January to March), rapid increases of air
301 temperature from below –30°C up to –0.2°C (e.g., 18 February), were observed. In
302 springtime (from April to June), the air temperature increased continuously, and from 1
303 June, air temperatures were near 0°C, although rapid increases (and subsequent
304 decreases) of air temperature to near 0°C were observed on two occasions in mid-May
305 (Cohen et al., 2017).

306

307

308 ## 3.2 Characteristics of snow, sea ice, and frost flowers

309

310 The snow and ice thickness at the observation sites ranged between 0.0 and 60.0 cm and
311 between 15.0 and >200 cm, respectively (Table 1). The thin snow and ice represent
312 newly formed ice in leads at station YI1. The thickness of the frost flowers ranged from
313 1.0 to 2.5 cm.

314

315 Figure 5 shows vertical profiles of snow and ice temperature and salinity in the top 20
316 cm of ice. Temperatures within the snowpack depended on the air temperature at the
317 time of observation. However, the bottom of the snow and the surface of the sea ice
318 were relatively warm (T>–7.5°C), except for the frost flowers station YI1 and the multi-
319 year ice station OI1 (Figure 5a and Table 2). High salinities (S>18.6) characterized the
320 bottom of the snow and the surface of the sea ice, except for the multi-year ice station
321 OI1 (Figure 5b). At the multi-year ice station OI1, salinity was zero through the snow
322 and top of sea ice. Salinity of frost flowers was up to 92.8 for the thin ice station YI1
323 (Figure 5b). Snow density and water equivalent ranged from 268 to 400 kg m^{-3} and 11
324 to 180 kg m^{-2}, respectively.

3.3 Physical and chemical properties of brine

The brine volume fraction, temperature, salinity, DIC, TA, and calculated pCO_2 are summarized in Table 2. Brine volume fraction in top 20 cm of ice was from 9 to 17%, except for the value of 0% at the multi-year ice station OI1 (Table 2). Brine temperatures and salinity ranged from −5.3 to −3.3°C and 51.8 to 86.6, respectively. DIC and TA of brine ranged from 3261 to 4841 μmol kg^{-1} and 3518 to 5539 μmol kg^{-1}, respectively. The pCO_2 of brine ($pCO_{2\,b}$) (334−693 μatm) was generally higher than that of atmosphere ($pCO_{2\,a}$) (401 ± 7 μatm), except for station FI4.

3.4 CO_2 flux

Table 3 summarizes the CO_2 flux measurements for each surface condition. For undisturbed natural surface conditions, i.e. measurements directly on the snow surface (F_{snow}) or the frost flowers (F_{ff}) on young ice, the mean CO_2 flux was +0.2 ± 0.2 mmol C m^{-2} day^{-1} for F_{snow} and +1.0 ± 0.6 mmol C m^{-2} day^{-1} for F_{ff}. The potential flux in cases when snow or frost flowers had been removed (F_{ice}) was +2.5 ± 4.3 mmol C m^{-2} day^{-1}. The air–sea ice CO_2 fluxes measured over the ice surface (F_{ice}) increased with increasing difference in pCO_2 between brine and atmosphere ($\Delta pCO_{2\,b-a}$) with significant correlation ($R^2 = 0.9$, $p < 0.02$), but this was not the case for F_{snow} ($R^2 = 0.0$, $p < 0.96$) (Figure 6).

4 Discussion

4.1 Effect of snow cover on the physical properties of sea ice surface

In this study, we examined CO_2 fluxes between sea ice and atmosphere in a variety of air temperature conditions from –32 to –3°C and diverse snow and ice conditions (Table 2). The bottom of the snow pack and the surface of the sea ice remained relatively warm (>–7.5°C) (Figure 5a, Table 2), except for stations OI1 and YI1, even though air temperature was sometimes below –40°C (Figure 4). Relatively warm ice temperatures were likely due to the upward heat transport from the bottom of the ice and in some cases the thick insulating snow cover, except for stations OI1 and YI1 (Table 2). Therefore, snow acted as thermal insulator over sea ice, and in general the snow depths observed during N-ICE2015 point towards this being representative for first-year and second-year or older ice in the study region in winter 2015 (Rösel et al., 2018). The young and first-year ice surfaces were characterized by high salinities (Figure 5b). During sea ice formation, upward brine transport to the snow pack occurs (e.g., Toyota et al., 2011). In addition, brine within the sea ice was not completely drained as compared to that of multi-year ice. Furthermore, formation of frost flowers and subsequent wicking up of surface brine into the frost flowers also provides high salinity at the surface of sea ice (Kaleschke et al., 2004; Geilfus et al., 2013; Barber et al., 2014; Fransson et al., 2015) as observed in this study (S>92) (Figure 5b). Snowfall over the frost flowers would have preserved the high salinity at the bottom of snow pack and top of sea ice for young and first-year ice.

As a result of the combination of the relatively high temperature and high salinity at the top of sea ice, brine volume fractions in the upper parts of the sea ice were high, up to 17% (Table 2). It has been shown that ice permeability increases by an order of magnitude when brine volume fraction > 5%, which would correspond to a temperature of –5°C for a bulk ice salinity of 5 – the so called “law of fives” (Golden et al., 1998; Pringle et al., 2009; Zhou et al., 2013). Because sea ice temperatures were low and thereby reduced permeability in winter season, generally, air–sea ice CO_2 flux is at its minimum in the winter (e.g., Delille et al., 2014). However, in our study, the brine volume fractions were generally >9%, except for station OI1 with fresh ice at the surface, providing conditions for active gas exchange within sea ice and between sea ice and atmosphere. This situation was likely made possible due to the thick snow cover and relatively thin and young sea ice.

388
389
390 **4.2 CO_2 fluxes over different sea-ice surface types**
391
392 The CO_2 flux measurements over different surface conditions indicate that the snow
393 cover over sea ice affects the magnitude of air–sea ice CO_2 flux, especially for stations
394 FI5 and FI6 (Table 3). For undisturbed natural surface conditions, the CO_2 flux
395 measured directly over snow-covered first-year ice and young ice with frost flowers
396 (F_{snow} and F_{ff}) was lower in magnitude than that for potential flux obtained directly over
397 the ice surface after removing snow (F_{ice}), especially for stations FI5, FI6, and YI1.
398
399 F_{ff} indicates that the frost flowers surface on young thin ice is a CO_2 source to the
400 atmosphere and F_{ff} was higher than F_{snow}, except for station FI1. Frost flowers are
401 known to promote gas flux, such as CO_2, from the sea ice to the atmosphere (Geilfus et
402 al., 2013; Barber et al., 2014; Fransson et al., 2015). At multi-year ice station OI1,
403 neither snow or ice surface acted as a CO_2 source/sink. The surface of multi-year ice did
404 not contain any brine (Figure 5b and Table 2), and the top of the ice was clear, colorless
405 and very hard, suggesting superimposed formation at the top of sea ice. This situation
406 would be similar as for freshwater-ice and superimposed-ice as these non-porous media
407 block gas exchange effectively at the sea ice surface (Delille et al., 2014). Snow-ice and
408 superimposed-ice were frequently found in second-year ice cores during N-ICE2015
409 (Granskog et al., 2017), so the 'blocking' of gas exchange in second-year and multi-
410 year ice may be a widespread process in the Arctic.
411
412 The magnitude of positive F_{snow} is less than F_{ice} for stations FI5 and FI6 (Table 3)
413 indicating that the potential CO_2 flux from sea ice decreased due to the presence of
414 snow. Previous studies have shown that snow accumulation over sea ice effectively
415 impede CO_2 exchange (Nomura et al., 2013; Brown et al., 2015). Nomura et al. (2013)
416 reported that 50–90% of the potential CO_2 flux was reduced due to the presence of
417 snow/superimposed-ice at the water equivalent of 57–400 kg m^{-2}, indicating that the
418 snow properties are an important factor that controls the CO_2 exchange through a
419 snowpack. Comparisons between stations FI5 and FI6 for F_{snow}/F_{ice} ratio (0.2 for FI5

and 0.0 for FI6) and water equivalent (11 kg m^{-2} for FI5 and 127 kg m^{-2} for FI6) indicate that the potential CO_2 flux is reduced (80% for FI5 and 98% for FI6 of the potential CO_2 flux) with increasing water equivalent. Although the magnitude of the potential CO_2 flux through the sea ice surface decreased by the presence of snow for stations FI5 and FI6 (Table 3), the snow surface still presents a CO_2 source to the atmosphere for low snow density and shallow depth conditions (e.g., +0.6 mmol C m^{-2} day^{-1} for FI5).

For F_{ice}, there were negative CO_2 fluxes at stations FI3 and FI4 (–0.6 mmol C m^{-2} day^{-1} for FI3 and –0.8 mmol C m^{-2} day^{-1} for FI4) (Table 3). These fluxes corresponded to low or negative$\Delta pCO_{2\ b-a}$ as compared to that in atmosphere (Table 2 and Figure 6). Negative CO_2 fluxes should correspond to negative $\Delta pCO_{2\ b-a}$. Therefore, the uncertainty for the calculation of carbonate chemistry may be one reason for the discrepancy in pCO_2 calculation in these conditions (Brown et al., 2014).

4.3 Comparison to earlier studies on sea-ice to air CO_2 flux

The CO_2 fluxes measured over the undisturbed natural surface conditions (F_{snow} and F_{ff}) in this study ranged from +0.1 to +1.6 mmol C m^{-2} day^{-1} (Table 3), which are at the lower end of the reported range based on the chamber method and eddy covariance method for natural and artificial sea ice (–259.2 to +74.3 mmol C m^{-2} day^{-1}) (Zemmelink et al., 2006; Nomura et al., 2006, 2010a, 2010b, 2013; Miller et al., 2011; Papakyriakou and Miller, 2011; Geilfus et al., 2012, 2013; 2014; Barber et al., 2014; Delille et al., 2014; Sørensen et al., 2014; Brown et al., 2015; Kotovitch et al., 2016). Direct comparison to previous studies is complicated because CO_2 flux measurements with both chamber and eddy covariance techniques were used during different condition for season and ice surface characteristics. In addition, discrepancies between chamber and eddy covariance measurements of air-ice CO_2 fluxes have been repeatedly observed. The footprint size of CO_2 exchange measured with the two approaches (Zemmelink et al., 2006, 2008; Burba et al., 2008; Amiro, 2010; Miller et al., 2011; Papakyriakou and Miller, 2011; Sørensen et al., 2014; Miller et al., 2015) may be one reason for the large

452 difference. The eddy covariance method reflects a flux integrated over a large area, that
453 can contain several different surface types. Therefore, eddy-covariance appears to be
454 more useful for understanding fluxes at large special and temporal scales. On the other
455 hand, the chamber method reflects the area where chamber was covered, and it is useful
456 for understanding the relationship between fluxes and ice surface conditions on smaller
457 scales. The different spatial scales of the two methods may be therefore one reason for
458 the discrepancy in CO_2 flux measurements.
459
460 Comparison of the natural CO_2 flux range (+0.1 to +1.6 mmol C m^{-2} day^{-1} for F_{snow} and
461 F_{ff}) (Table 3) with previous estimates derived from the chamber method (–5.2 to +6.7
462 mmol C m^{-2} day^{-1}) (Nomura et al., 2006, 2010a, 2010b, 2013; Geilfus et al., 2012,
463 2013; 2014; Barber et al., 2014; Delille et al., 2014; Brown et al., 2015; Kotovitch et al.,
464 2016) (these studies include both natural and potential fluxes) shows that CO_2 fluxes
465 during NICE2015 experiment are at the lower end of positive values. However, our
466 potential CO_2 flux (F_{ice}) was a larger CO_2 source (up to +11.8 mmol C m^{-2} day^{-1}) than
467 reported in previous studies (+6.7 mmol C m^{-2} day^{-1}). In our study, the maximum
468 potential flux (e.g., +11.8 mmol C m^{-2} day^{-1}) was obtained for F_{ice} at station FI6 (Table
469 3). In this situation, $\Delta pCO_{2\ b-a}$ (293 μatm) was the highest (Table 2 and Figure 6), and it
470 is reasonable to consider this as the highest magnitude of positive CO_2 flux within our
471 study. However, a previous study by closed chamber method showed that even for a
472 similar $\Delta pCO_{2\ b-a}$ (297 μatm) and magnitude for the brine volume fraction (10–15%),
473 the CO_2 flux was +0.7 mmol C m^{-2} day^{-1} for artificial sea ice with no snow in the tank
474 experiment (Nomura et al., 2006).
475
476 The CO_2 flux between the sea ice and overlying air can be expressed by the following
477 equation,
478
479 $F_{CO2} = r_b\ k\ \alpha\ \Delta pCO_{2\ b-a}$,
480
481 where r_b is the ratio of surface of the brine channel to sea ice surface, and we assume
482 that the value of r_b is equal to brine volume fraction, k is the gas transfer velocity, α is
483 the solubility of CO_2 (Weiss, 1974), and $\Delta pCO_{2\ b-a}$ is the difference in pCO_2 between

brine and atmosphere. The equation is based on the fact that CO_2 transfer between seawater and air is controlled by processes in the near-surface water (Liss, 1973). The gas transfer velocity (k) calculated from F, r_b, α and $\Delta pCO_{2\ b-a}$ was 5.12 m day^{-1} for F_{ice} at station FI6 and 0.29 m day^{-1} for the tank experiment examined in Nomura et al. (2006). This result clearly indicates that the gas transfer velocity for F_{ice} at station FI6 is higher than that of tank experiment examined in Nomura et al. (2006) even with very similar $\Delta pCO_{2\ b-a}$ and brine volume fraction.

Here, we surmise that the gas transfer velocity and thereby CO_2 flux is greatly enhanced by the temperature difference between sea ice surface and atmosphere. Previous studies indicate that there is an unstable air density gradient in a dry snowpack due to basal heating and the strong temperature difference develops between bottom and top of snow (e.g., Powers et al., 1985; Severinghaus et al., 2010), which enhances the flow of air through the snowpack. We propose that the mixing and transport of gas within the snowpack could also occur over sea ice. Because temperatures at the bottom of snow and the top of sea ice were relatively warm due to a thick insulating snow over sea ice, there was a strong temperature difference between sea ice surface and atmosphere when air temperature was low (Figure 5a and Table 2). For station FI6, temperature difference between sea ice surface and atmosphere was 20.2°C after snow removal. On the other hand, in the tank experiment by Nomura et al. (2006), the temperature difference between sea ice surface (top 1.5 cm) and air in the headspace was only 4.5°C.

Figure 6 shows the relationship between mean air–sea ice CO_2 fluxes and temperature difference between ice and atmosphere. The strong dependence of CO_2 flux with temperature difference (T_{ice}–T_a) was observed, especially for F_{ff} and F_{ice} ($R^2 > 0.7$, $p < 0.01$) (Figure 6). Due to the high brine volume fractions (Table 2), sea ice surface had enough permeability for gas exchange. In addition, ice temperatures were similar for young and first-year ice (Figure 6, Table 2), indicating that pCO_2 at the top of sea ice and CO_2 flux would be of similar order of magnitude if thermodynamic processes dominated. Therefore, our results suggest that the CO_2 fluxes even over the frost flowers as a natural condition, would be enhanced by the upward transport of air containing high CO_2 from the surface of sea ice to the atmosphere due to the strong

temperature difference between sea ice surface and atmosphere. Although the presence of snow on sea ice has potential to produce a larger temperature difference between sea ice surface and atmosphere and promote the upward transport, the magnitude of the CO_2 flux decreased due to the presence of snow. However, for young sea ice with frost flowers (e.g., station YI1), ice surface temperature was warm (Table 2), suggesting that CO_2 flux would be enhanced by the large temperature difference between sea ice surface and atmosphere.

5 Conclusions

We measured CO_2 fluxes along with sea ice and snow physical and chemical properties over first-year and young sea ice north of Svalbard in the Arctic pack ice. Our results suggest that young thin snow-free ice, with or without frost flowers, is a source of atmospheric CO_2 due to the high pCO_2 and salinity and relatively high sea ice temperature. Although the potential CO_2 flux from sea-ice surface decreased due to the presence of snow, snow surface still presents a modest CO_2 source to the atmosphere for low snow density and shallow depth situations. The highest ice to air fluxes were observed over thin young sea ice formed in leads. During N-ICE2015 the ice pack was dynamic, and formation of open water was associated with storms, where new ice was formed. The subsequent ice growth in these leads becomes important for the ice-to-air CO_2 fluxes in winter due to the fact that the flux from young ice is an order of magnitude larger than from snow-covered first-year and older ice.

6 Data availability

Data used in this paper will be available at Norwegian Polar Data Centre (data.npolar.no).

7 Acknowledgments

We would like to express heartfelt thanks to the crew of R/V Lance and all members of the N-ICE2015 expedition for their support in conducting the field work. This work was supported by the Japan Society for the Promotion of Science (#15K16135, #24-4175), Research Council of Norway (KLIMAFORSK programme, grant 240639), the Centre of Ice, Climate and Ecosystems (ICE) at the Norwegian Polar Institute through the N-ICE project, the Ministry of Climate and Environment and the Ministry of Foreign Affairs of Norway and the Grant for Joint Research Program of the Institute of Low Temperature Science, Hokkaido University. AF, MC and MAG were supported by the flagship research program "Ocean acidification and ecosystem effects in Northern waters" within the FRAM-High North Research Centre for Climate and the Environment. BD is a research associate of the F.R.S-FNRS.

Reference list

Amiro, B.: Estimating annual carbon dioxide eddy fluxes using open-path analysers for cold forest sites. Agr. Forest Meteorol., 150, 15, 1366–1372. 2010.

Bain, W. G., Hutyra, L., Patterson, D. C., Bright, A. V.,Daube, B. C. Munger, J. W., Wofsy, S. C.: Wind-induced error in the measurement of soil respiration using closed dynamic chambers. Agricul. Forest Meteo., 131, 3–4, 225–232, 2005.

Barber, D. G., Ehn, J. K., Pućko, M., Rysgaard, S., Deming, J. W. and co-authors: Frost flowers on young Arctic sea ice: The climatic, chemical and microbial significance of an emerging ice type. J Geophys. Res.-Atmos. doi: 10.1002/2014JD021736. 2014.

579 Brown, K. A, Miller, L. A., Davelaar, M., Francois, R., and Tortell P. D.: Over-
580 determination of the carbonate system in natural sea ice brine and assessment of
581 carbonic acid dissociation constants under low temperature, high salinity conditions.
582 Mar. Chem 165: 36–45. doi: 10.1016/j.marchem.2014.07.005. 2014.
583
584 Brown, K. A., Miller, L.A., Mundy, C. J., Papakyriakou, T., Francois, R., and co-
585 authors: Inorganic carbon system dynamics in landfast Arctic sea ice during the early-
586 melt period. J. Geophys. Res. Oceans, 120, 3542–3566.
587 http://dx.doi.org/10.1002/2014JC010620. 2015.
588
589 Burba, G., McDermitt, D., Grelle, A., Anderson, D., and Xu, L.: Addressing the
590 influence of instrument surface heat exchange on the measurements of CO_2 flux from
591 open-path gas analyzers, Global Change Biol., 14, 8, 1854–1876, 2008.
592
593 Cohen, L., Hudson, S. R., Walden, V. P., Graham, R. M., and Granskog, M. A.:
594 Meteorological conditions in a thinner Arctic sea ice regime from winter through
595 summer during the Norwegian young sea ICE expedition (N-ICE2015), J. Geophys. Res.
596 Atmos., 122, 7235–7259, doi:10.1002/2016JD026034, 2017.
597
598 Cox, G. F. N., and Weeks W. F.: Equations for determining the gas and brine volumes
599 in sea-ice samples, J. Glaciol., 29, 306–316, 1983.
600
601 Delille, B., Jourdain, B., Borges, A. V., Tison, J.-L., and Delille, D.: Biogas (CO_2, O_2,
602 dimethylsulfide) dynamics in spring Antarctic fast ice, Limnol. Oceanogr., 52, 1367–
603 1379, 2007.
604
605 Delille, B., Vancoppenolle, M., Geilfus, N.-X.. Tilbrook, B. Lannuzel.D., and co-
606 authors: Southern Ocean CO_2 sink: the contribution of the sea ice, J. Geophys. Res.
607 Oceans. 119 (9), 6340–6355, 2014.
608
609 Dickson, A. G., and Millero F. J.: A comparison of the equilibrium constants for the
610 dissociation of carbonic acid in seawater media, Deep-Sea Res. 34, 1733–1743, 1987.

611
612 Dickson, A. G.: Thermodynamics of the dissociation of boric acid in synthetic seawater
613 from 273.15 to 318.15 K, Deep-Sea Res. 37, 755–766, 1990.
614
615 Dickson, A. G., Sabine, C. L., and Christian, J. R. Eds.: Guide to Best Practices for
616 Ocean CO_2 Measurements, PICES Special Publication, 3, 191 pp, 2007.
617
618 Fransson, A., Chierici, M., Miller, L. A., Carnat, G., Thomas, H., and co-authors:
619 Impact of sea ice processes on the carbonate system and ocean acidification state at the
620 ice-water interface of the Amundsen Gulf, Arctic Ocean, J. Geophys. Res., 118, 1–23,
621 doi:10.1002/2013JC009164, 2013.
622
623 Fransson, A., Chierici, M., Abrahamsson, K., Andersson, M., Granfors, A., and co-
624 authors: CO_2-system development in young sea ice and CO_2 gas exchange at the ice/air
625 interface mediated by brine and frost flowers in Kongsfjorden, Spitsbergen, Ann.
626 Glaciol., 56, 69, doi: 10.3189/2015A0G69A563, 2015.
627
628 Fransson, A., Chierici, M., Skjelvan, I., Olsen, A., Assmy, P., Peterson, A. K., Ward,
629 B.: Effects of sea-ice and biogeochemical processes and storms on under-ice water f
630 CO_2 during the winter-spring transition in the high Arctic Ocean: Implications for sea-
631 air CO_2 fluxes, J. Geophys. Res. Oceans, 122(7), 5566–5587.
632 https://doi.org/10.1002/2016JC012478. 2017.
633
634 Geilfus, N.-X., Carnat, G., Papakyriakou, T., Tison, J.-L., Else, B. and co-authors:
635 Dynamics of pCO_2 and related air–ice CO_2 fluxes in the Arctic coastal zone (Amundsen
636 Gulf, Beaufort Sea), J. Geophys. Res., 117, C00G10, doi:10.1029/2011JC007118, 2012.
637
638 Geilfus, N.-X., Carnat, G., Dieckmann, G. S., Halden, N., Nehrke, G., and co-authors:.
639 First estimates of the contribution of $CaCO_3$ precipitation to the release of CO_2 to the
640 atmosphere during young sea ice growth, J. Geophys. Res., 118:244–255.
641 http://dx.doi.org/10.1029/2012JC007980, 2013.
642

643 Geilfus, N.-X., Tison, J.-L., Ackley, S. F., Galley, R. J., Rysgaard, S., and co-authors:
644 Sea ice pCO_2 dynamics and air–ice CO_2 fluxes during the Sea Ice Mass Balance in the
645 Antarc-tic (SIMBA) experiment – Bellingshausen Sea, Antarctica, The Cryosphere, 8,
646 2395–2407, doi:10.5194/tc-8-2395-2014, 2014.
647
648 Geilfus, N.-X., Galley, R. J., Crabeck, O., Papakyriakou, T., Landy, J., Tison, J.-L. and
649 Rysgaard, S.: Inorganic carbon dynamics of melt-pond-covered first-year sea ice in the
650 Canadian Arctic, Biogeosci., 12, 2047–2061, doi:10.5194/bg-12-2047-2015, 2015.
651
652 Gleitz, M., Vonderlo, M. R., Tomas, D. N., Dieckmann, G. S. and Millero F. J.:
653 Comparison of summer and winter inorganic carbon, oxygen and nutrient
654 concentrations in Antarctic sea ice brine, Mar. Chem., 51, 81–89, 1995.
655
656 Golden, K. M., Ackley, S. F. and Lytle, V. I.: The percolation phase transition in sea ice,
657 Science, 282, 2238–2241, 1998.
658
659 Granskog, M. A., Assmy, P., Gerland, S., Spreen, G., Steen, H., and co-authors: Arctic
660 research on thin ice: Consequences of Arctic sea ice loss, Eos Transactions AGU, 97,
661 22–26, doi:10.1029/2016EO044097, 2016.
662
663 Granskog, M. A., Rösel, A., Dodd, P. A., Divine, D., Gerland, S., and co-authors: Snow
664 contribution to first-year and second-year Arctic sea ice mass balance north of Svalbard,
665 J. Geophys. Res. Oceans, 122, 2539-2549, doi: 10.1002/2016JC012398, 2017.
666
667 Hudson, S. R., Cohen, L., and Walden, V.: N-ICE2015 surface meteorology (Data set),
668 Norwegian Polar Institute, doi: 10.21334/npolar.2015.056a61d1, 2015.
669
670 Inoue, H. Y. and Ishii M.: Variations and trends of CO_2 in the surface seawater in the
671 Southern Ocean south of Australia between 1969 and 2002, Tellus, Ser. B, 57, 58–69,
672 2005.
673

674 Jonas, T., Marty, C., and Magnusson, J.: Estimating the snow water equivalent from
675 snow depth measurements in the Swiss Alps, J. Hydrol., 378, 161–167, 2009.
676
677 Kaleschke, L., Richter, A., Burrows, J., Afe, O., Heygster, G., and co-authors: Frost
678 flowers on sea ice as a source of sea salt and their influence on tropospheric halogen
679 chemistry, Geophys. Res. Lett., 31, L16114, doi:10.1029/2004GL020655, 2004.
680
681 Kotovitch, M., Moreau, S., Zhou, J., Vancoppenolle, M., Dieckmann, G. S., and co-
682 authors: Air–ice carbon pathways inferred from a sea ice tank experiment, Elementa:
683 Science of the Anthropocene, 4, 1, doi10.12952/journal.elementa.000112, 2016.
684
685 Lindsay, R., and Schweiger, A.: Arctic sea ice thickness loss determined using
686 subsurface, aircraft, and satellite observations, The Cryosphere, 9(1), 269–283,
687 doi:10.5194/tc-9-269-2015, 2015.
688
689 Liss, P. S.: Processes of gas exchange across an air-water interface, Deep-Sea Res. 20,
690 221–238, 1973.
691
692 Massman, W., Sommerfeld, R., Zeller, K., Hehn, T., Hudnell, L., and Rochelle, S.: CO_2
693 flux through a Wyoming seasonal snowpack: diffusional and pressure pumping effects,
694 Biogeochemistry of Seasonally Snow-Covered Catchments (Proceedings of a Boulder
695 Symposium, July 1995). IAHS Publ., 228, 71–79, 1995.
696
697 Massom, R.A., Eicken, H., Haas, C., Jeffries, M. O., Drinkwater, M. R., and other co-
698 authors: Snow on Antarctic sea ice, Reviews of Geophysics, 39, 413–445, 2001.
699
700 Mehrbach, C., Culberson, C. H., Hawley, J. E., and Pytkowicz P. M.: Measurement of
701 the apparent dissociation constant of carbonic acid in seawater at atmospheric pressure,
702 Limnol. Oceanogr., 18, 897–907, 1973.
703
704 Meier, W. N., Hovelsrud, G. K., van Oort, B. E. H., Key, J. R., Kovacs, K. M., and co-
705 authors: Arctic sea ice in transformation: A review of recent observed changes and

706 impacts on biology and human activity, Rev. Geophys., 52, 185–217,
707 doi:10.1002/2013RG000431, 2014.
708
709 Miller, L. A., Papakyriakou, T. N., Collins, R. E., Deming, J. W., Ehn, J. K., and co-
710 authors: Carbon dynamics in sea ice: A winter flux time series, J. Geophys. Res., 116,
711 C02028, doi:10.1029/2009JC006058, 2011.
712
713 Miller, L. A., Fripiat, F., Else, B. G. T., Bowman, J. S., Brown, K. A., and co-authors:.
714 Methods for Biogeochemical Studies of Sea Ice: The State of the Art, Caveats, and
715 Recommendation, Elementa, 3, 000038, doi:10.12952/journal.elementa.000038, 2015.
716
717 Nomura, D., Inoue, H. Y., and Toyota, T.: The effect of sea-ice growth on air–sea CO_2
718 flux in a tank experiment, Tellus, Ser. B, 58, 418–426, 2006.
719
720 Nomura, D., Inoue, H. Y., Toyota, T., and Shirasawa, K.: Effects of snow, snowmelting
721 and refreezing processes on air–sea-ice CO_2 flux, J. Glaciol., 56, 196, 262–270, 2010a.
722
723 Nomura, D., Eicken, H., Gradinger, R., and Shirasawa, K.: Rapid physically driven
724 inversion of the air-sea ice CO_2 flux in the seasonal landfast ice off Barrow, Alaska
725 after onset of surface melt, Cont. Shelf Res., 30, 1998–2004, 2010b.
726
727 Nomura, D., Granskog, M. A., Assmy, P., Simizu, D., and Hashida, G.: Arctic and
728 Antarctic sea ice acts as a sink for atmospheric CO_2 during periods of snow melt and
729 surface flooding, J. Geophys. Res. Oceans, 118, 6511–6524, 2013.
730
731 Merkouriadi, I., Gallet, J.-C., Graham, R. M., Liston, G. E., Polashenski, C., Rösel, A.,
732 and Gerland, S.: Winter snow conditions on Arctic sea ice north of Svalbard during the
733 Norwegian young sea ICE (N-ICE2015) expedition, J. Geophys. Res. Atmos., 122,
734 doi:10.1002/2017JD026753, 2017.
735
736 Papadimitriou, S., Kennedy, H., Norman, L., Kennedy, D. P., Dieckmann, G. S., and
737 co-authors: The effect of biological activity, $CaCO_3$ mineral dynamics, and CO_2

738 degassing in the inorganic carbon cycle in sea ice in late winter-early spring in the
739 Weddell Sea, Antarctica, J. Geophys. Res. 117, C08011, doi:10.1029/2012JC008058,
740 2012.
741
742 Papakyriakou, T., and Miller, L. A.: Springtime CO_2 exchange over seasonal sea ice in
743 the Canadian Arctic Archipelago, Ann. Glaciol., 52, 57, 215–224, 2011.
744
745 Parmentier, F. J. W., Christensen, T. R., Sørensen, L. L., Rysgaard, S., McGuire, A. D.,
746 and co-authors: The impact of lower sea-ice extent on Arctic greenhouse-gas exchange,
747 Nature Climate Change, 3, 195–202, doi:10.1038/nclimate1784, 2013.
748
749 Petrich, C. and Eicken, H.: Growth, structure and properties of sea ice, in Thomas, D. N.
750 and Dieckmann, G. S. eds., Sea Ice, 2nd ed., Oxford, Wiley-Blackwell, 23–77, 2010.
751
752 Pierrot, D., Lewis, E. and Wallace, D. W. R.: MS Excel Program Developed for CO_2
753 System Calculations, ORNL/CDIAC-105a. Carbon Dioxide Information Analysis
754 Center, Oak Ridge National Laboratory, U.S. Department of Energy, Oak Ridge,
755 Tennessee, doi: 10.3334/CDIAC/otg.CO2SYS_XLS_CDIAC105a, 2006.
756
757 Powers, D., Oneill, K., and Colbeck, S. C.: Theory of natural convection in snow, J.
758 Geophys. Res.-Atmos., 90, 10641–10649, doi:10.1029/Jd090id06p10641, 1985.
759
760 Pringle, D. J., Miner, J. E., Eicken, H., and Golden, K. M.: Pore space percolation in sea
761 ice single crystals, J. Geophys. Res., 114, C12017, doi:10.1029/2008JC005145, 2009.
762
763 Rysgaard, S., Søgaard, D. H., Cooper, M., Pucko, M., Lennert, K., and co-authors:
764 Ikaite crystal distribution in winter sea ice and implications for CO_2 system dynamics,
765 The Cryosphere, 7, 707–718, doi:10.5194/tc-7-707-2013, 2013.
766
767 Rösel, A., Itkin, P., King, J., Divine, D., Wang, C., Granskog, M. A., Krumpen, T. and
768 Gerland, S.: Thin Sea Ice, Thick Snow, and Widespread Negative Freeboard Observed

During N-ICE2015 North of Svalbard, J. Geophys. Res. Oceans, 123(2), 1156–1176, doi:10.1002/2017JC012865, 2018.

Schindlbacher, A., Zechmeister-Boltenstern, S., Glatzel, G., and Jandl R.: Winter soil respiration from an Austrian mountain forest, Agric, For. Meteorol., 146, 205–215, doi:10.1016/j.agrformet.2007.06.001, 2007.

Severinghaus, J. P., Albert, M. R., Courville, Z. R., Fahnestock, M. A., Kawamura, K., and co-authors: Deep air convection in the firn at a zero-accumulation site, central Antarctica, Earth Planet. Sci. Lett., 293, 359–367, doi:10.1016/J.Epsl.2010.03.003, 2010.

Stroeve, J. C., Serreze, M. C., Holland, M. M., Kay, J. E., Maslanik, J., and Barrett, A. P.: The Arctic's rapidly shrinking sea ice cover: a research synthesis, Climatic Change, 110, 1005, doi:10.1007/s10584-011-0101-1, 2012.

Sørensen, L. L, Jensen, B., Glud, R. N., McGinnis, D. F., and Sejr, M. K.: Parameterization of atmosphere-surface exchange of CO_2 over sea ice, The Cryosphere, 8: 853–866. doi:10.5194/tc-8-853-2014, 2014.

Takagi, K., Nomura, M., Ashiya, D., Takahashi, H., Sasa, K., and co-authors: Dynamic carbon dioxide exchange through snowpack by wind-driven mass transfer in a conifer-broadleaf mixed forest in northernmost Japan, Global Biogeochem. Cycles, 19, GB2012, doi:10.1029/2004GB002272, 2005.

Toyota, T., Massom, R., Tateyama, K., Tamura, T., and Fraser, A.: Properties of snow overlying the sea ice off East Antarctica in late winter 2007, Deep Sea Res. II, 58, 1137–1148, 2011.

Vancoppenolle, M., Meiners, K. M., Michel, C., Bopp, L., Brabant, F., and co-authors: Role of sea ice in global biogeochemical cycles: emerging views and challenges, Quat. Sci. Rev., 79, 207–230, 2013.

Weiss, R. F.: Carbon dioxide in water and seawater: the solubility of a non-ideal gas, Mar. Chem., 2, 203–215, 1974.

Zemmelink, H. J., Delille, B., Tison, J.-L., Hintsa, E. J., Houghton, L., and co-authors:. CO_2 deposition over the multi-year ice of the western Weddell Sea, Geophys. Res. Lett., 33, L13606, doi:10.1029/2006GL026320, 2006.

Zemmelink, H. J., Dacey, J. W. H., Houghton, L., Hintsa. E. J., and Liss, P. S.: Dimethylsulfide emissions over the multi-year ice of the western Weddell Sea, Geophys. Res. Lett., 35, L06603, doi:10.1029/2007GL031847, 2008.

Zhou, J., Delille**,** B., Eicken, H., Vancoppenolle, M., Brabant, F., and co-authors: Physical and biogeochemical properties in landfast sea ice (Barrow, Alaska): Insights on brine and gas dynamics across seasons, J. Geophys. Res. 118, 6, 3172–3189, 2013.

Figure captions

Figure 1. Location map of the sampling area north of Svalbard during N-ICE2015. Image of the sea ice concentrations (a) and station map (b) were derived from Special Sensor Microwave Imager (SSM/I) satellite data for mean of February 2015 and from Sentinel-1 (Synthetic Aperture Radar Sensor) satellite data, respectively.

Figure 2. Photographs of the CO_2 flux chamber system at station YI1 north of Svalbard on Friday 13 March 2015. CO_2 flux chamber was installed over the frost flowers on the new thin ice in the refreezing lead.

Figure 3. Example of the temporal variation in CO_2 concentration (ΔCO_2) in the chambers installed at station YI1 that is use to calculate the CO_2 flux. ΔCO_2 indicates the change in CO_2 concentration inside the chamber since the chamber was closed.

Figure 4. Time series of air temperature measured at the weather mast over the ice floe (10 m height) (Hudson et al., 2015). Blank period indicates no data. Colored symbols indicate the date for the chamber flux measurements. The horizontal dashed line indicates air temperature = 0°C.

Figure 5. Vertical profiles of temperature (a) and salinity (b) in snow and sea ice (top 20 cm). The horizontal line indicates snow–ice interface. Shaded area indicates sea ice. The triangle in (a) indicates the air temperature for each station. For stations FI7 and YI2 and 3, we have no salinity data.

Figure 6. Relationships between mean air–sea ice CO_2 fluxes and temperature difference between ice (T_{ice}) and atmosphere (T_a) (circle) and ice temperature (Tice) (top 20 cm) (cross) for F_{snow} (blue), F_{ff} (black) and F_{ice} (red) for young and first-year sea ice. Relationships between mean air–sea ice CO_2 fluxes and the difference of pCO_2 ($\Delta pCO_{2\ b–a}$) between brine ($pCO_{2\ b}$) and atmosphere ($pCO_{2\ a}$) (triangle) for F_{snow} (solid gray) and F_{ice} (open gray).

Table captions

Table 1. Station, date for CO_2 flux measurement, position, floe number, surface condition, ice type and thickness of snow, frost flowers, and sea ice.

a. Sea ice coring and snow sampling was conducted on 5 March 2015.

b. Sea ice coring and snow sampling was conducted on 10 March 2015.

Table 2. Station, snow density and water equivalent, brine volume fraction, and temperature for sea ice (top 20 cm), brine temperature, salinity, DIC, TA, pCO_2 ($pCO_{2\ b}$), and atmospheric temperature, wind speed, pCO_2 ($pCO_{2\ a}$)[a] and $\Delta pCO_{2\ b–a}$.

865

866 a. $pCO_{2\,a}$ (µatm) was calculated from CO_2 concentration (ppmv) at Ny-Ålesund,
867 Svalbard (http://www.esrl.noaa.gov/gmd/dv/iadv/) taking into account saturated water
868 vapor and atmospheric pressure during sampling day.
869

870 b. Mean values for snow column.
871

872 c. "–" indicates no data. Due to technical reasons, data of snow, sea ice, and brine were
873 not obtained.
874
875

876 Table 3. CO_2 flux measured over the snow (F_{snow}), frost flowers (F_{ff}), and ice surface
877 (F_{ice}). Values measured directly over undisturbed surfaces (either with frost flowers or
878 on snow surface) at a given station are indicated in bold.
879

880 a. Data of first CO_2 flux measurement after removal of snow or frost flowers.
881

882 b. "–" indicates no data.
883

884 c. Number of measurements in bracket.
885

886 d. Data from station OI1 was not included.

Table 1. Station, position, date for CO_2 flux measurement, floe number, surface condition, ice type and thickness of snow, frost flower, and sea ice.

Station	Position	Date of 2015	Floe number	Surface condition	Ice type[c]	Thickness (cm)		
						Snow	Frost flower	Sea ice
FI1	83º03.77N, 17º34.94E	28 January	1	Frost flower	First-year ice	0.0	1.0	37.0
FI2	83º03.77N, 17º34.94E	28 January	1	Snow	First-year ice	8.0	No	35.0
FI3	83º08.00N, 24º09.02E	5 and 8 March[a]	2	Snow	First-year ice	29.0	No	98.0
FI4	83º10.56N, 22º09.42E	9 March	2	Snow	First-year ice	36.0	No	92.0
FI5	83º06.02N, 21º38.29E	10 and 11 March[b]	2	Snow	First-year ice	3.0	No	48.0
FI6	82º55.36N, 21º25.92E	12 March	2	Snow	First-year ice	37.0	No	69.0
FI7	81º22.18N, 08º59.93E	13 May	3	Snow	First-year ice	26.5	No	127.0
YI1	82º52.52N, 21º16.54E	13 March	2	Frost flower	Young ice	0.0	1.0	15.0
YI2	81º46.53N, 13º16.00E	5 May	3	Snow and frost flower mixed	Young ice	2.5	2.5	17.5
YI3	81º32.45N, 11º17.20E	9 May	3	Snow and frost flower mixed	Young ice	2.0	2.0	22.0
OI1	83º07.18N, 24º25.59E	6 March	2	Snow	Old ice (multi-year ice)	60.0	No	>200

a. Sea ice coring, brine and snow sampling was conducted on 5 March 2015.

b. Sea ice coring, brine and snow sampling was conducted on 10 March 2015.

c. Ice type was categorized based on WMO (1970).

Table 2. Station, snow density and water equivalent, brine volume fraction and temperature for sea ice (top 20 cm), brine temperature, salinity, DIC, TA, pCO_2 ($pCO_{2\,b}$) and atmospheric temperature, wind speed, pCO_2 ($pCO_{2\,a}$)[a] and $\Delta pCO_{2\,b-a}$.

Station	Snow		Sea ice (top 20 cm)		Brine					Atmosphere			
	Density[b] ($kg\ m^{-3}$)	Water equivalent ($kg\ m^{-2}$)	Brine volume fraction (%)	Temperature (ºC) (range)	Temperature (ºC)	Salinity	DIC ($\mu mol\ kg^{-1}$)	TA ($\mu mol\ kg^{-1}$)	$pCO_{2\,b}$ (µatm)	Temperature (ºC)	Wind speed ($m\ second^{-1}$)	$pCO_{2\,a}$ (µatm)	$\Delta pCO_{2\,b-a}$ (µatm)
FI1	–[c]	–[c]	–[c]	–[c]	–[c]	–[c]	–[c]	–[c]	–[c]	−31.6	4.0	405	–[c]
FI2	–[c]	–[c]	–[c]	–[c]	–[c]	–[c]	–[c]	–[c]	–[c]	−31.6	4.0	405	–[c]
FI3	399	104	9	−6.8 (−7.4 to −6.3)	−5.2	84.8	4628	5539	427	−3.3	9.0	400	27
FI4	400	180	9	−4.7 (−5.5 to −3.7)	−5.3	86.6	4433	5490	334	−3.5	6.2	386	−52
FI5	268	11	17	−3.5 (−3.8 to −3.1)	−3.3	51.8	3261	3518	472	−18.1	6.8	389	83
FI6	343	127	13	−4.8 (−5.7 to −3.8)	−4.8	84.0	4841	5493	693	−25.0	3.6	400	293
FI7	–[c]	–[c]	–[c]	−6.1 (−6.1 to −5.8)	–[c]	–[c]	–[c]	–[c]	–[c]	−13.0	5.8	405	–[c]
YI1	–[c]	–[c]	17	−6.6 (−12.3 to −2.6)	–[c]	–[c]	–[c]	–[c]	–[c]	−26.0	2.6	402	–[c]
YI2	–[c]	–[c]	–[c]	−3.6 (−5.1 to −1.8)	–[c]	–[c]	–[c]	–[c]	–[c]	−16.2	4.5	407	–[c]
YI3	–[c]	–[c]	–[c]	−3.9 (−6.4 to −2.0)	–[c]	–[c]	–[c]	–[c]	–[c]	−14.2	6.7	410	–[c]
OI1	–[c]	–[c]	0	−10.8 (−11.0 to −10.9)	–[c]	–[c]	–[c]	–[c]	–[c]	−13.5	4.7	397	–[c]

a. $pCO_{2\,a}$ (µatm) was calculated from CO_2 concentration (ppmv) at Ny-Ålesund, Svalbard (http://www.esrl.noaa.gov/gmd/dv/iadv/) taking into account the saturated water vapor and atmospheric pressures at sampling day.

b. Mean values for column.

c. "–" indicates no data. Due to the technical reason, data of snow, sea ice, and brine were not obtained.

Table 3. CO_2 flux measured over the snow (F_{snow}), frost flowers (F_{ff}) and ice surface (F_{ice}).

Station	CO_2 flux (mmol C m^{-2} day^{-1})		
	Natural flux (mean ± 1SD)		Potential flux
	F_{snow}	F_{ff}	F_{ice} [a]
FI1	–[b]	**+0.1 ± 0.1** (n=7)c	–[b]
FI2	**+0.4 ± 0.3** (n=13)[c]	–[b]	–[b]
FI3	**+0.1 ± 0.1** (n=7)[c]	–[b]	−0.6
FI4	**+0.1 ± 0.1** (n=6)[c]	–[b]	−0.8
FI5	**+0.6 ± 0.3** (n=5)[c]	–[b]	+2.6
FI6	**+0.2 ± 0.1** (n=5)[c]	–[b]	+11.8
FI7	**+0.1 ± 0.1** (n=10)[c]	–[b]	±0.0
YI1	–[b]	**+1.6 ± 0.2** (n=6)[c]	+7.3
YI2	–[b]	**+1.3 ± 0.2** (n=9)[c]	+1.0
YI3	–[b]	**+1.0 ± 0.4** (n=8)[c]	+1.1
OI1	**+0.1 ± 0.0** (n=6)[c]	–[b]	+0.2
Mean[d]	**+0.2 ± 0.2** (n=46)[c]	**+1.0 ± 0.6** (n=30)[c]	+2.5 ± 4.3 (n=9)[c]

a. Data of first measurement after removal of snow or frost flower.

b. "–" indicates no data.

c. Number of measurements in bracket.

d. Data of station OI1 was not included.

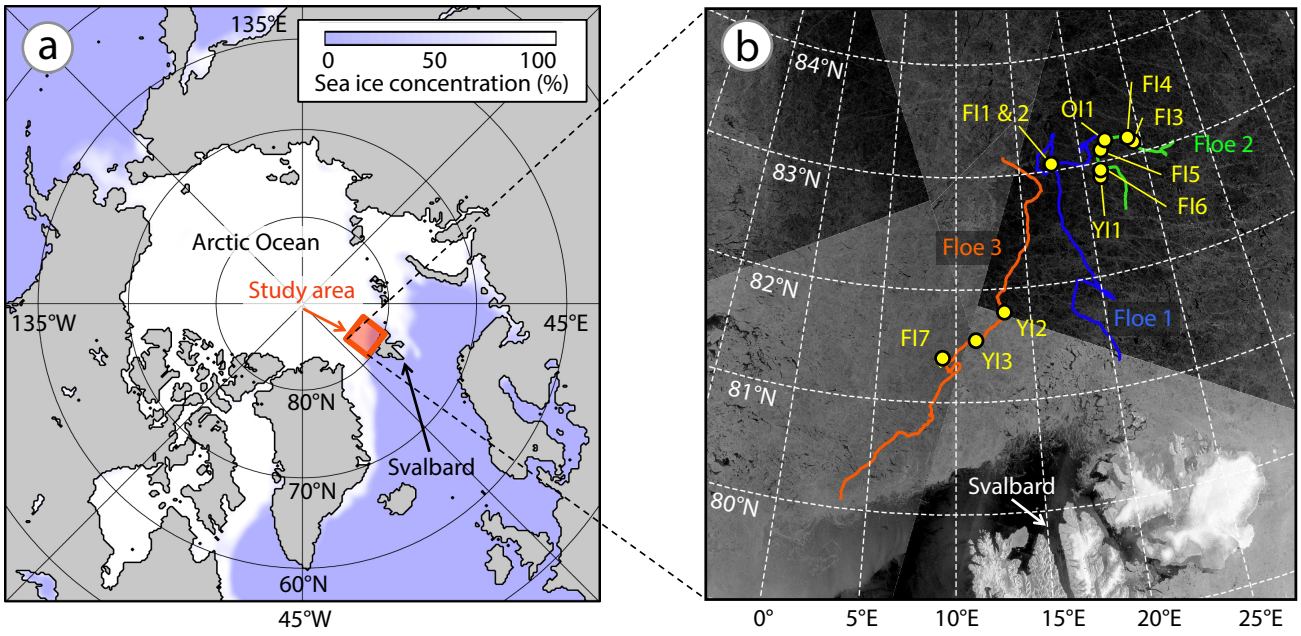

Nomura et al., Figure 1 (Double column size)

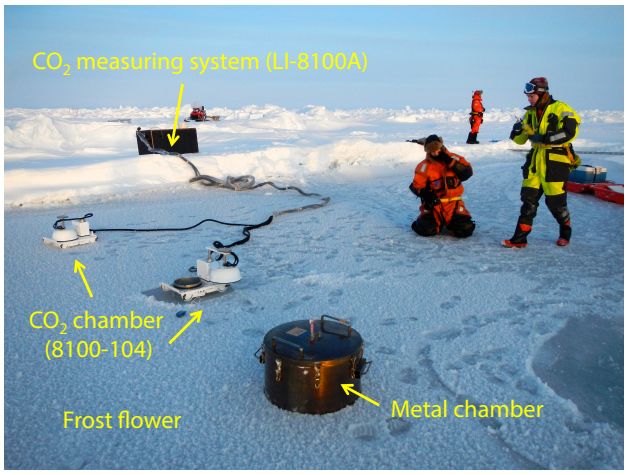

Nomura et al., Figure 2 (Single column size)

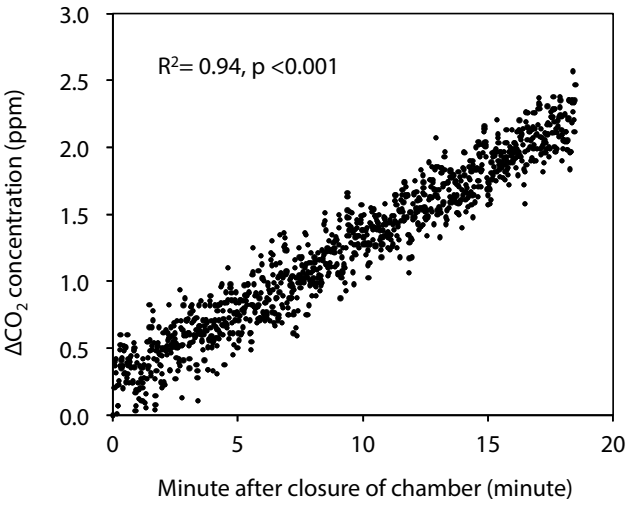

Nomura et al., Figure 3 (Single column size)

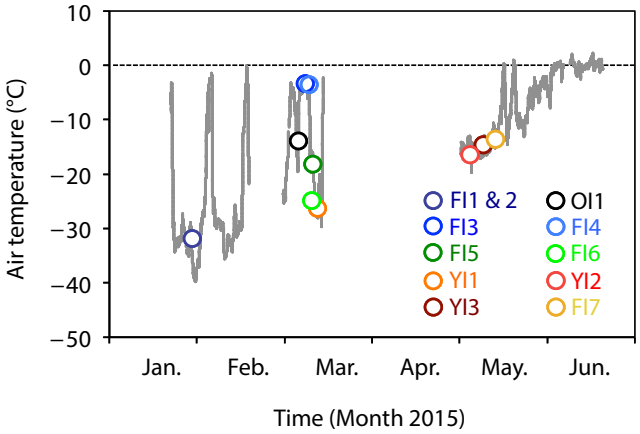

Nomura et al., Figure 4 (Single column size)

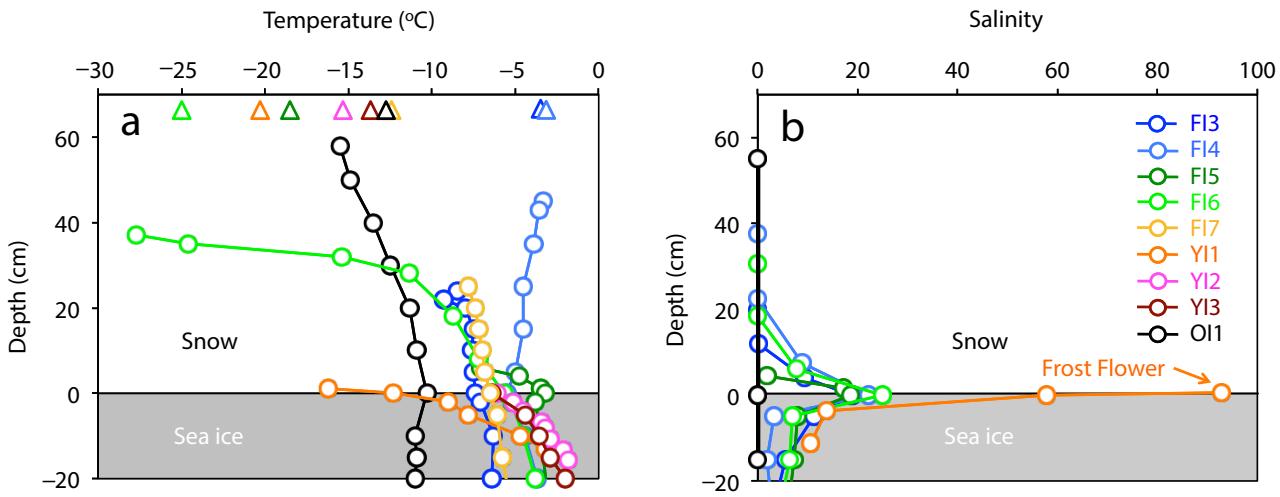

Nomura et al., Figure 5 (Double column size)

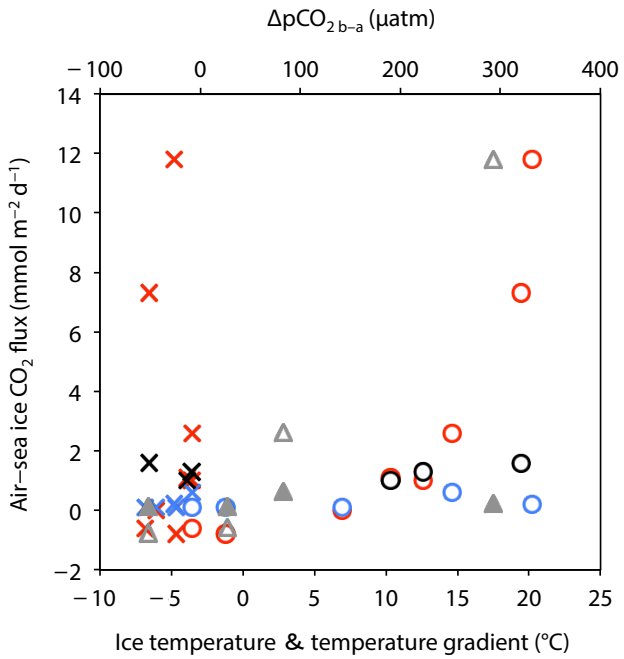

Nomura et al., Figure 6 (Single column size)